Process modeling of composites by resin transfer molding: practical applications of sensitivity analysis for isothermal considerations

Received November 2001
Revised January 2003
Accepted January 2003

B.J. Henz
US Army Research Laboratory, Aberdeen Proving Grounds, MD, USA

K.K. Tamma and R. Kanapady
Department of Mechanical Engineering and Army High Performance Computing Research Center, University of Minnesota, Minneapolis, MN, USA

N.D. Ngo
University of Minnesota, Minneapolis, MN, USA

P.W. Chung
US Army Research Laboratory, Aberdeen Proving Grounds, MD, USA

Keywords *Sensitivity analysis, Resins, Moulding, Finite elements*

Abstract *The resin transfer molding process for composites manufacturing consists of either of two considerations, namely, the fluid flow analysis through a porous fiber preform where the location of the flow front is of fundamental importance, and the combined flow/heat transfer/cure analysis. In this paper, the continuous sensitivity formulations are developed for the process modeling of composites manufactured by RTM to predict, analyze, and optimize the manufacturing process. Attention is focused here on developments for isothermal flow simulations, and various illustrative examples are presented for sensitivity analysis of practical applications which help serve as a design tool in the process modeling stages.*

The authors are very pleased to acknowledge the support in part by Battelle/US Army Research Office (ARO), Research Triangle Park, NC, under grant number DAAH04-96-C-0086, and by the US Army High Performance Computing Research Center (AHPCRC) under the auspices of the Department of the Army, US Army Research Laboratory (ARL) cooperative agreement number DAAH04-95-2-0003/contract number DAAH04-95-C-0008. The content does not necessarily reflect the position or the policy of the government, and no official endorsement should be inferred. Support in part by Dr Andrew Mark of the Integrated Modeling and Testing (IMT) Computational Technical Activity and the ARL/Major Shared Resource Center (MSRC) facilities is also gratefully acknowledged. Special thanks are due to the Computational and Information Sciences Directorate (CISD) and the Materials Division at ARL, Aberdeen Proving Ground, MD. Other related support in form of computer grants from the Minnesota Supercomputer Institute (MSI), Minneapolis, MN, is also gratefully acknowledged.

International Journal of Numerical Methods for Heat & Fluid Flow
Vol. 13 No. 4, 2003
pp. 415-447

0961-5539
DOI 10.1108/09615530310475894

1. Introduction

In manufacturing processes there are many factors that affect the resulting product. Many times, the job of an engineer is to find the best process by weighing the various input factors and their effect on the outcome. In the recent past the optimization method has changed from heuristic trial-and-error to more rigorous computational methods employing the finite element method (FEM). Trial-and-error is still used with the FEM, but only the computer time is involved and costly trial runs and experiments can be eliminated. A more stringent method for optimizing manufacturing processes which does not require the level of intuition as trial-and-error is via sensitivity analysis. With properly designed software the engineer can define the limits of input parameters and through iteration and optimization an optimal solution is computed.

For a parametrized state system, the so-called sensitivity analysis involves taking the partial derivative of state variables with respect to the problem parameters. In this regard, the sensitivity analysis serves as a useful design tool. In general, sensitivity analysis is the study of how sensitive the outcome of process is to variations of given input parameters. Such analysis of sensitivity can be conducted as a parametric study or through the so-called continuous sensitivity equation (CSE) as described in this paper. Various applications of sensitivity analysis are available in the literature and are typical of metal forming, heat transfer, structural optimization, shape design, and the like (Blackwell *et al.*, 1999a, b; Gantar and Kuzman, 2002; Gelin and Labergere, 2002; Ghouati *et al.*, 2000; Navarrina *et al.*, 2000).

A practical and useful application of interest in this paper is that related to advanced manufacturing of composites process modeling using the resin transfer molding (RTM) process. The process involves impregnating the complex fabric preforms with a polymer resin and the manufactured part is removed from the mold after completely wetting the preform and curing is complete. Such composite structural parts are widely used in military, automotive and civilian applications because of the several inherent advantages of composites manufactured by such process. For the RTM process, some effort has gone into optimization and sensitivity analysis but this work has concentrated mostly on parametric studies for sensitivity analysis and genetic algorithms for optimization (Chui *et al.*, 1997; Jiang *et al.*, 2001; Kim *et al.*, 2002). Some preliminary work to develop and implement the CSE for RTM filling appears in the literature (Henz *et al.*, 2000, 2002; Mathur *et al.*, 2002). In comparison to existing status of the efforts, in this paper, further advancements in the applications of sensitivity analysis studies is undertaken for RTM process based on the CSE representation. In particular, from a practical viewpoint and to serve as a design tool, the developments help optimize fill time, gate locations, determination of unknown material properties, etc.

In this study, the CSE is formulated for RTM process modeling of composites. Attention is focused here on isothermal situations which is an acceptable practice for significantly large molds and helps serve a useful purpose for preliminary design stages. Essentially, the physical problem is that of the resin flow through a porous fiber network and the accurate tracking of the moving fluid flow front. The CSE approach is useful for design as it starts from the original governing model equations and with the FEM of discretization, the system of finite element sensitivity equations are formulated and solved. It happens that this system of sensitivity equations is always linear; and also, that they can be solved as a post-processing phase so that the computational requirements and code modifications are minimal. After the CSE is formulated for the isothermal RTM filling model, the results are used to analyze and verify a sample problem. The sensitivity analysis results are applied to a variety of simulations to include the determination of a variable material property, such as permeability or viscosity and compared with experimental results, and also for predicting the optimal injection parameters for a complex structural geometries of composite part.

In the following, we briefly first summarize the pure finite element formulation of the resin transfer mold filling process for iso-thermal situations for tracking the fluid flow fronts. Next, we discuss the CSE formulation and the corresponding numerical implementation for sensitivity analysis. Finally, we present examples in which the CSE is employed, in particular, for optimizing the filling time of RTM mold filling process and its related applications.

2. Isothermal RTM

2.1 Governing equations

Under certain circumstances, such as in the case of relatively large molds, the assumption of isothermal flow is reasonable for use in RTM. In this paper, the sensitivity formulations are described wherein both the pressure and fill time sensitivities are investigated. In the isothermal RTM mold filling, the pressure sensitivity, $S_P \equiv \partial P/\partial p$, where p is the sensitivity parameter, with respect to inlet flow rate q, permeability $\overline{\mathbf{K}}$, and viscosity μ, also, the fill time sensitivity, $S_{t_{\text{fill}}} \equiv \partial t_{\text{fill}}/\partial p$, with respect to inlet pressure P_0, permeability, viscosity, and inlet location x are studied. The governing model equations for isothermal RTM process modeling are briefly described next.

Continuity:

$$\frac{\partial \rho}{\partial t} + \nabla \cdot (\rho \mathbf{u}) = 0 \tag{1}$$

Employing the Gauss theorem to convert the volume integral to a surface integral, we have

$$\int_{\Omega} \frac{\partial \rho}{\partial t} \, d\Omega + \int_{\Gamma} \rho(\mathbf{u} \cdot \mathbf{n}) \, d\Gamma = 0 \tag{2}$$

From practical considerations and to provide improved physical attributes over existing approaches, it is possible to track the flow front following an implicit pure finite element mold filling formulation as described by Mohan *et al.* (1998, 1999) and Ngo *et al.* (1998). Here a variable Ψ, namely the fill factor, is introduced as

$$\int_{\Omega} \frac{\partial}{\partial t}(\rho \Psi) \, d\Omega + \int_{\Gamma} \rho \Psi(\mathbf{u} \cdot \mathbf{n}) \, d\Gamma = 0 \tag{3}$$

Using the product rule on the first term of equation (3), and the fact that for an incompressible flow, $\frac{\partial \rho}{\partial t} = 0$, it yields

$$\int_{\Omega} \rho \frac{\partial \Psi}{\partial t} \, d\Omega + \int_{\Gamma} \rho \Psi(\mathbf{u} \cdot \mathbf{n}) \, d\Gamma = 0 \tag{4}$$

or equivalently, for an incompressible fluid the result is given as

$$\int_{\Omega} \frac{\partial \Psi}{\partial t} \, d\Omega + \int_{\Gamma} \Psi(\mathbf{u} \cdot \mathbf{n}) \, d\Gamma = 0 \tag{5}$$

Applying the Gauss theorem to the second term of equation (5), yields the representation

$$\int_{\Omega} \frac{\partial \Psi}{\partial t} \, d\Omega + \int_{\Omega} \Psi \nabla \cdot \mathbf{u} \, d\Omega = 0 \tag{6}$$

Moving the velocity term to the right hand side yields

$$\int_{\Omega} \frac{\partial \Psi}{\partial t} \, d\Omega = - \int_{\Omega} \Psi \nabla \cdot \mathbf{u} \, d\Omega \tag{7}$$

Darcy's Law is given as

$$\mathbf{u} = - \frac{\overline{\mathbf{K}}}{\mu} \cdot \nabla \mathbf{P} \tag{8}$$

where $\overline{\mathbf{K}}$ is the permeability tensor of the fiber preform which is defined appropriately for two and three-dimensional preform considerations. Upon substituting equation (8) into equation (7), the transient filling model equation is given as

$$\int_{\Omega} \frac{\partial \Psi}{\partial t} \, d\Omega = \int_{\Omega} \Psi \nabla \cdot \left(\frac{\overline{\mathbf{K}}}{\mu} \cdot \nabla P \right) d\Omega \tag{9}$$

It should be noted here that the viscosity is not a function of temperature, and hence the isothermal nature of the model. The boundary conditions for equation (9) are given as follows

$$\begin{aligned} &\frac{\partial P}{\partial \mathbf{n}} = 0 \ \text{on mold walls} \\ &P = 0 \ \text{at flow front} \\ &P = P_0 \ \text{prescribed pressure at inlet or} \\ &q = q_0 \ \text{prescribed flow rate at inlet} \end{aligned} \tag{10}$$

where $\mathbf{n}$ is the normal to the progressing flow front, and P_0 and q_0 represent pressure and flow rate at the inlet(s), respectively. The two initial conditions ($t = 0$) required to solve equation (9) are given as

$$\Psi = 1 \quad \text{at inlet} \quad \Psi = 0 \quad \text{elsewhere} \tag{11}$$

At this point it should be noted that the pressure gradient at the unfilled nodes is negligible. This implies that equation (9) is only solved for the completely filled nodes (i.e. $\Psi = 1$). Hence,

$$\int_\Omega \frac{\partial \Psi}{\partial t} \, \mathrm{d}\Omega = \int_\Omega (1) \nabla \cdot \left(\frac{\overline{\mathbf{K}}}{\mu} \cdot \nabla P \right) \mathrm{d}\Omega \tag{12}$$

2.2 Finite element procedure

In order to solve the isothermal problem, the FEM is employed as

$$\int_\Omega \mathbf{W}^{\mathrm{T}} \frac{\partial \Psi}{\partial t} \, \mathrm{d}\Omega = \int_\Omega \mathbf{W}^{\mathrm{T}} \left(\nabla \cdot \frac{\overline{\mathbf{K}}}{\mu} \cdot \nabla \mathbf{P} \right) \mathrm{d}\Omega \tag{13}$$

Applying the Gauss-Green formula to equation (13) yields

$$\int_\Omega \mathbf{W}^{\mathrm{T}} \frac{\partial \Psi}{\partial t} \, \mathrm{d}\Omega + \int_\Omega \nabla \mathbf{W}^{\mathrm{T}} \frac{\overline{\mathbf{K}}}{\mu} \cdot \nabla P \, \mathrm{d}\Omega = \int_\Gamma \mathbf{W}^{\mathrm{T}} \frac{\overline{\mathbf{K}}}{\mu} \cdot \nabla P \, \mathrm{d}\Gamma \tag{14}$$

The weighting functions, $\mathbf{W}$, are chosen as the element shape functions $\mathbf{N}$. Both the pressure and fill factors are approximated as

$$\mathbf{PM} = \sum_{i=1}^{n_n} N_i P_i \quad \mathbf{\Psi} = \sum_{i=1}^{n_n} N_i \Psi_i \tag{15}$$

where n_n is the number of nodes in the finite element mesh. After introducing equation (15), equation (14) can be represented as the following finite element semi-discretized equation system

$$\mathbf{C}\dot{\mathbf{\Psi}} + \mathbf{K}\mathbf{P} = \mathbf{q} \tag{16}$$

where

$$\begin{aligned}
\mathbf{C} &= \int_{\Omega} \mathbf{N}^{\mathrm{T}}\mathbf{N}\,\mathrm{d}\Omega \\
\mathbf{K} &= \int_{\Omega} \mathbf{B}^{\mathrm{T}}\frac{\overline{\mathbf{K}}}{\mu}\mathbf{B}\,\mathrm{d}\Omega \\
\mathbf{q} &= \int_{\Gamma} \mathbf{N}^{\mathrm{T}}\left(\frac{\overline{\mathbf{K}}}{\mu}\cdot\nabla P\cdot\mathbf{n}\right)\mathrm{d}\Gamma \\
\dot{\mathbf{\Psi}} &= \frac{\mathbf{\Psi}_{n+1} - \mathbf{\Psi}_n}{\Delta t}
\end{aligned} \tag{17}$$

Substituting the definition for $\dot{\mathbf{\Psi}}$ from equation (17) into equation (16) yields

$$\mathbf{C}[\Psi_{n+1} - \Psi_n] + \Delta t\mathbf{K}\mathbf{P} = \Delta t\mathbf{q} \tag{18}$$

and the fill factor and pressure solutions are obtained through an iterative technique as described in Mohan *et al.* (1998, 1999) and Ngo *et al.* (1998), for the implicit formulations employed here.

2.3 Computational procedure

Since equation (18) is the pertinent discretized model equation in the present methodology, the fill factors and the pressure for the values associated with the nodes are solved for in an iterative manner. At the beginning of the simulation the fill factors are known and are taken to be unity at the injection nodes. Then at each time step, values for the pressure field and the fill factor are iteratively computed until a mass conservation is reached. Convergence in the pressure and fill solutions are ensured during the iteration process by following the strict criteria

$$P = \begin{cases} 0 & \text{for} \quad \psi < 1 \\ P_{\text{calculated}} & \text{for} \quad \psi = 1 \end{cases} \tag{19}$$

and by accounting for the overflowing and underflowing of the fill factor ψ. Below is a step-by-step procedure of the iterative technique used in the present implicit pure FE methodology of computation:

(1) At the beginning of each time step, set

$$\{\psi_i\}_m^{n+1} = \{\psi_i\}^n \tag{20}$$

where subscript m refers to the mth iteration, and superscripts n and n+1 are the previous and current time step, respectively.

(2) Form lumped mass matrix **C**, stiffness matrix **K**, and load vector **q** using equation (17). If the finite element mesh of the discretized domain does not change throughout the simulation, the mass matrix **C** should only be computed once and stored for subsequent usage.

(3) Apply prescribed and fill boundary conditions to stiffness matrix **K**.
- Prescribed boundary condition: $P = P_0$ or $q = q_0$ at injection ports.
- Fill boundary condition: $P = 0$ at nodes where $\psi < 1$. Note that by definition, the flow front is assumed to exist in regions where $0 < \psi < 1$.

(4) Form modified load vector **g** using

$$\{g_i\}_m = C_{ii}\{\psi_i\}^n - C_{ii}\{\psi_i\}_m^{n+1} + \Delta t\{q_i\}_m \tag{21}$$

where subscript i refers to the ith node, C_{ii} is the ith component of the lumped matrix **C**, and q_i is the ith component of the load vector **q**.

(5) Solve the system of equations

$$[\hat{K}_{ij}]_m\{P_j\}_m = \{g_i\}_m \tag{22}$$

where $\hat{K}_{ij}$ is the aforementioned matrix **K** after application of prescribed and fill boundary conditions.

(6) Compute the new nodal resin fraction field $\{\psi_i\}_{m+1}^{n+1}$ using the discrete mass balance equation,

$$C_{ii}\{\psi_i\}_{m+1}^{n+1} = C_{ii}\{\psi_i\}^n - \Delta t[K_{ij}]_m\{P_j\}_m + \Delta t\{q_i\}_m \tag{23}$$

Note that only a matrix vector product and two vector additions are performed in this calculation.

(7) Since the fill factor ψ of a particular node cannot be greater than 1 (e.g. over-filling) or less than 0 (e.g. under-filling), the computed value of ψ is corrected by

$$\{\psi_i\}_{m+1}^{n+1} = \max\left[0, \min\left(1, \{\psi_i\}_{m+1}^{n+1}\right)\right] \tag{24}$$

(8) Check for convergence of resin mass between two consecutive iterations using

$$\left|C_{ii}\{\psi_i\}_{m+1}^{n+1} - C_{ii}\{\psi_i\}_m^{n+1}\right| \leq \varepsilon \tag{25}$$

(9) If convergence is not reached, reset the iteration counter m and the fill factor solution

$$\{\psi_i\}_m^{n+1} = \{\psi_i\}_{m+1}^{n+1} \tag{26}$$

and perform another iteration by looping back to Step 2. If convergence is reached, proceed to the next time step.

3. Sensitivity analysis

In this section, the CSE is developed for isothermal RTM filling applications including sensitivity of parameters such as permeability, viscosity, inlet pressure, inlet flow rate, and inlet location. A cost function is then developed to compute the fill time of the mold so that the fill time sensitivity can be computed. Finally, the sensitivity results are verified with the use of a derived analytical solution and subsequently some numerical examples are presented.

3.1 CSE

The sensitivity equation for the RTM filling is derived by taking the partial derivative of Darcy's Law, given by equation (8), which is subsequently coupled with the continuity equation, equation (1), with respect to the sensitivity parameter p, resulting in the quasi-steady state equation for mold filling. This equation is employed here rather than the implicit pure finite element formulation shown earlier as it more directly relates to the sensitivity analysis. Thus,

$$\nabla \cdot \left(\frac{\overline{\mathbf{K}}}{\mu} \cdot \nabla P \right) = 0 \tag{27}$$

Note that equation (27) is a quasi steady-state representation. This implies that the time steps are restricted according to stability considerations when solving the RTM filling problem. The boundary conditions for equation (27) are the same as those given in equation (10). The next step for solving the sensitivity is to compute the CSE for isothermal RTM filling. The CSE is obtained by taking the partial derivative of equation (27) and the associated boundary conditions given by equation (10) with respect to an arbitrary sensitivity parameter p. Thus

$$\frac{\partial}{\partial p} \left(\nabla \cdot \left(\frac{\overline{\mathbf{K}}}{\mu} \cdot \nabla P \right) \right) = 0 \tag{28}$$

After using the chain-rule to obtain the derivatives of all terms, equation (28) becomes

$$\nabla \cdot \left[\frac{\partial \overline{\mathbf{K}}}{\partial p} \frac{1}{\mu} \cdot \nabla P + \overline{\mathbf{K}} \frac{\partial}{\partial \mathbf{p}} \left(\frac{1}{\mu} \right) \cdot \nabla \mathbf{P} + \frac{\overline{\mathbf{K}}}{\mu} \cdot \nabla \mathbf{S}_{\mathrm{P}} \right] = 0 \tag{29}$$

The associated boundary conditions for equation (29) are given as

$$\begin{aligned}
&\frac{\partial}{\partial p}\left(\frac{\partial P}{\partial \mathbf{n}}\right) = 0 \quad \text{on mold walls} \\
&\frac{\partial P}{\partial p} = 0 \quad \text{at flow front} \\
&\frac{\partial P}{\partial p} = \frac{\partial P_0}{\partial p} \quad \text{for constant pressure at inlet} \\
&\frac{\partial q}{\partial p} = \frac{\partial q_0}{\partial p} \quad \text{for constant flow rate at inlet}
\end{aligned} \tag{30}$$

The boundary conditions for equation (29) can be rewritten, from equation (30), using the definition of pressure sensitivity $S_P \equiv \partial P/\partial p$, as

$$\begin{aligned}
&\frac{\partial S_P}{\partial \mathbf{n}} = 0 \text{ on mold walls} \\
&S_P = 0 \text{ at flow front} \\
&S_P = \frac{\partial P_0}{\partial p} \text{ for constant pressure at inlet} \\
&S_q = \frac{\partial q_0}{\partial p} \text{ for constant flow rate at inlet}
\end{aligned} \tag{31}$$

where the flow rate sensitivity is defined as $S_q \equiv \partial q/\partial p$. If the sensitivity parameter is the inlet location then the boundary conditions are represented as

$$\begin{aligned}
&\frac{\partial S_P}{\partial \mathbf{n}} = 0 \quad \text{on mold walls} \\
&S_P = 0 \quad \text{at flow front} \\
&S_P = -\frac{\partial P}{\partial x} \quad \text{at inlet}
\end{aligned} \tag{32}$$

The inlet boundary condition from equation (32), is found by using the chain rule in the following manner

$$\frac{\partial P(x(p);p)}{\partial p} = \frac{\partial P}{\partial p} + \frac{\partial P}{\partial x}\frac{\partial x}{\partial p} = \frac{\partial P_0}{\partial p} \tag{33}$$

Since $\partial P_0/\partial p = 0$ and $\partial x/\partial p = 1$, equation (32) is obtained.

3.2 Finite element formulation

Employing the method of weighted residuals to derive the finite element equations, equation (29) leads to

$$\int_\Omega \mathbf{W}^{\mathrm{T}}\nabla\cdot\left(\frac{\partial\overline{\mathbf{K}}}{\partial p}\frac{1}{\mu}\cdot\nabla P + \overline{\mathbf{K}}\frac{\partial}{\partial p}\left(\frac{1}{\mu}\right)\cdot\nabla P + \frac{\overline{\mathbf{K}}}{\mu}\cdot\nabla S_P\right)\mathrm{d}\Omega = 0 \tag{34}$$

Applying the Gauss-Green formula to equation (34), yields

$$\begin{aligned}&\int_\Omega \nabla\mathbf{W}^{\mathrm{T}}\frac{\partial\overline{\mathbf{K}}}{\partial p}\frac{1}{\mu}\cdot\nabla P\,\mathrm{d}\Omega + \int_\Omega \nabla\mathbf{W}^{\mathrm{T}}\overline{\mathbf{K}}\frac{\partial}{\partial p}\left(\frac{1}{\mu}\right)\cdot\nabla P\,\mathrm{d}\Omega + \int_\Omega \nabla\mathbf{W}^{\mathrm{T}}\frac{\overline{\mathbf{K}}}{\mu}\cdot\nabla S_P\,\mathrm{d}\Omega\\ &= \int_\Gamma \frac{1}{\mu}\mathbf{W}^{\mathrm{T}}\frac{\partial\overline{\mathbf{K}}}{\partial p}\cdot\nabla P\cdot n\,\mathrm{d}\Gamma + \int_\Gamma \mathbf{W}^{\mathrm{T}}\overline{\mathbf{K}}\frac{\partial}{\partial p}\left(\frac{1}{\mu}\right)\cdot\nabla P\cdot n\,\mathrm{d}\Gamma\\ &+ \int_\Gamma \mathbf{W}^{\mathrm{T}}\frac{\overline{\mathbf{K}}}{\mu}\cdot\nabla S_P\cdot n\,\mathrm{d}\Gamma = 0\end{aligned} \tag{35}$$

The weighting functions $\mathbf{W}$ are chosen to be the same as the element shape functions $\mathbf{N}$. Interpolating $\mathbf{S}_{\mathrm{P}}$ yields

$$\begin{aligned}\mathbf{S}_{\mathrm{P}} &= \sum_{i=1}^{n_n} N_i S_{P_i}\\ \mathbf{P} &= \sum_{i=1}^{n_n} N_i P_i\\ \mathbf{W} &= \mathbf{N}\end{aligned} \tag{36}$$

The sensitivity finite element equation is given in the following semi-discretized equation representation

$$\frac{\partial \mathbf{K}}{\partial p}\mathbf{P} + \mathbf{K}\mathbf{S}_{\mathbf{P}} = \mathbf{S}_{\mathrm{q}} \tag{37}$$

where $\partial \mathbf{K}/\partial p, \mathbf{K}$, and $\mathbf{S}_{\mathrm{q}}$ are defined as

$$\frac{\partial \mathbf{K}}{\partial p} = \int_{\Omega} \mathbf{B}^{\mathrm{T}} \frac{\partial \overline{\mathbf{K}}}{\partial p} \frac{1}{\mu} \mathbf{B}\, \mathrm{d}\Omega + \int_{\Omega} \mathbf{B}^{\mathrm{T}} \overline{\mathbf{K}} \left(-\frac{1}{\mu^2} \right) \frac{\partial \mu}{\partial p} \mathbf{B}\, \mathrm{d}\Omega \quad \mathbf{K} = \int_{\Omega} \mathbf{B}^{\mathrm{T}} \frac{\overline{\mathbf{K}}}{\mu} \mathbf{B}\, \mathrm{d}\Omega$$

$$\mathbf{S}_{\mathrm{q}} = \int_{\Gamma} \mathbf{N}^{\mathrm{T}} \frac{\partial \overline{\mathbf{K}}}{\partial p} \frac{1}{\mu} \cdot \nabla P \cdot \mathbf{n}\, \mathrm{d}\Gamma + \int_{\Gamma} \mathbf{N}^{\mathrm{T}} \overline{\mathbf{K}} \frac{\partial}{\partial p} \left(\frac{1}{\mu} \right) \cdot \nabla P \cdot \mathbf{n}\, \mathrm{d}\Gamma \tag{38}$$

$$+ \int_{\Gamma} \mathbf{N}^{\mathrm{T}} \frac{\overline{\mathbf{K}}}{\mu} \cdot \nabla S_P \cdot \mathbf{n}\, \mathrm{d}\Gamma$$

It is now possible to implement the RTM sensitivity equation. Note that in equation (37) the left-hand pressure term **P** is already known when the pressure sensitivity for the current time step is to be computed. This allows for the pressure sensitivity and pressure results to be computed in parallel, where pressure sensitivity is always one time step behind the pressure computations.

3.3 Computational procedure

The sensitivity equations can be solved with minimal changes to existing RTM software. The current simulations were executed employing the general purpose code on composite technology of polymeric useful structures (OCTOPUS). Only a few extra function calls need to be added to the existing code to compute the sensitivity results. The sensitivity equation to be solved is stated in equation (37) in conjunction with the boundary conditions given in equation (31). The solution procedure is outlined here, with the mold filling implicit pure finite element algorithm previously described in Mohan *et al.* (1998, 1999) and Ngo *et al.* (1998).

(1) Form the mass matrix, **C**, stiffness matrix, **K**, and the load vector, **q**, as defined in equation (17).

(2) Next, form the sensitivity stiffness matrix, $\partial \mathbf{K}/\partial p$, and the sensitivity load vector, $\mathbf{S}_{\mathrm{q}}$, as defined in equation (38). The parameters necessary for this are computed by taking the partial derivative of permeability, $\overline{\mathbf{K}}$, and viscosity, μ, with respect to the sensitivity parameter, p.

(3) Apply the natural boundary conditions. These are considered by stating that once a control volume is filled, the mass balance must be held, so $\mathbf{q} = \{0\}$ for all nodes.

(4) Apply the prescribed boundary conditions to the stiffness matrix, **K**, given in equation (10).

(5) Solve for the pressure distribution by solving the finite element equation, equation (18).

(6) Compute and apply the prescribed sensitivity inlet conditions from equation (31). This includes prescribed S_P or S_q at the mold inlets.

(7) Compute the pressure sensitivity distribution, $\mathbf{S}_P$, from equation (37).

(8) Save the results and continue on to the next time step, until the filling is completed.

4. Optimization

Cost functions are functions that describe a result derived from the computational procedure. Examples of these results could be the amount of porosity, shape of the flow front, or the fill time. The last of these, namely, the fill time, is chosen as an illustrative example for the isothermal RTM model simulations. The fill time is an important consideration in the RTM manufacturing process because it affects how much cure will occur before the mold is completely filled, which in turn affects the final structural properties of the part. The fill time also affects the rate at which parts are manufactured. The objective here is to derive a cost function for the RTM filling process and utilize the CSE results to analyze this cost function, namely, the fill time. This information can then be used later to optimize the computational model with respect to the sensitivity parameter, or to compute an unknown material property.

4.1 Cost function derivation

The fill time sensitivity is derived by first defining a function that includes the fill time and by taking the partial derivative with respect to the sensitivity parameter p and solving for $\partial t_{\text{fill}}/\partial p$, the fill time sensitivity. The information required to solve for the fill time sensitivity is then computed and finally the fill time sensitivity cost function is augmented to the computational procedure. For RTM, the pressure sensitivity, S_P, is first solved for in equation (37) using the FEM. In order to solve equation (37) the necessary boundary conditions must be applied. This includes the inlet conditions which may be constant pressure or constant flow rate and the natural boundary conditions which state that resin mass can neither be created nor destroyed inside the manufactured part. The pressure sensitivity value is then used to compute the flow rate sensitivity at the mold inlet(s), with equation (37), after which the fill time sensitivity is computed. The function used to evaluate mold fill time is given in equation (39) (Henz *et al.*, 2000) and is different to that described in Mathur *et al.* (2002) which does not consider the present integration limits arising from the use of the quasi-steady state governing model equation. The volume of the mold filled during each time step is computed as

$$V_{\Delta t} = \int_0^{\Delta t_f} q_{\text{inlet}}\, \mathrm{d}t \tag{39}$$

where q_{inlet} is the flow rate at the mold inlet, $V_{\Delta t}$ is the volume of mold filled during the current time step, and Δt_f is the length of the current time step. The volume of the mold filled is evaluated at each time step. As equation (27) is a quasi steady-state function it is only valid for a given time step. To compute the fill time sensitivity the partial derivative of equation (39) must be taken with respect to the sensitivity parameter p. Thus

$$\frac{\partial V_{\Delta t}}{\partial p} = \frac{\partial}{\partial p} \int_0^{\Delta t_f} q_{\text{inlet}}\, \mathrm{d}t \tag{40}$$

which yields

$$0 = \int_0^{\Delta t_f} S_{q_{\text{inlet}}}\, \mathrm{d}t + \frac{\partial \Delta t_f}{\partial p} q_{\text{inlet}}(\Delta t_f) \tag{41}$$

Solving for $\partial \Delta t_f / \partial p$ the fill time sensitivity for the current time step is defined as

$$\frac{\partial \Delta t_f}{\partial p} = \frac{\int_0^{\Delta t_f} S_{q_{\text{inlet}}}\, \mathrm{d}t}{q_{\text{inlet}}(\Delta t_f)} \tag{42}$$

which when summed over all the time steps, the fill time sensitivity, namely, the cost function is computed as

$$S_{t_f} = \sum_{\text{AllTimeSteps}} \frac{\int_0^{\Delta t_f} S_{q_{\text{inlet}}}\, \mathrm{d}t}{q_{\text{inlet}}(\Delta t_f)} \tag{43}$$

These results can be used for optimization, which for the current analysis is minimization of the fill time. The method used to minimize the fill time can include conjugate gradient search methods, genetic algorithms, and the like. With these methods the optimum value is computed for a given sensitivity parameter. In the present study the fill time optimization is not presented but the fill time sensitivity results are instead used to compute material properties and optimal boundary conditions.

4.2 Computational procedure

This discussion is focused on fill time optimization. It should be noted that other optimizations can be used for the RTM process including flow rate analysis, last points to fill, shape of the flow front, etc. Highlighted next is the computational procedure that is employed for optimization of the RTM process.

(1) Compute the sensitivity results for the process outcome of interest with respect to the sensitivity parameter(s), i.e. fill time sensitivity with respect to resin viscosity. This result is in fact the gradient of fill time with respect to the sensitivity parameters.

(2) Optimize the process outcome by use of the steepest descent for minimization, as described in Shewchuk (1994), or Newton iterations for desired results as in equation (52).

(3) Iterate using the optimization method of choice. Following this procedure is a discussion of the "golden section" (Press *et al.*, 2002) and steepest descent methods used for optimization of functions where the gradient is known, i.e. the sensitivity results.

(4) The output of the previous step is a guess of the processing parameter values required to optimize the RTM process. These parameter values are compared with the most recently utilized parameters and if they are the "same" or "sufficiently close" then the optimal parameters are known. When the processing parameter is geometric then the optimization procedure stops when the parameter values are the same. This is because the geometry has been discretized for the finite element analysis. If the processing parameter is a continuous function then a good stopping criterion is when the difference in value is no longer measurable by available methods.

The use of the combined steepest descent and golden section methods is discussed here for minimization of fill time with respect to inlet location, or any other case where multiple sensitivity parameters are used for the analysis. The geometry is assumed flat so that only the x and y directions are considered.

(1) Begin by selecting a node on the surface where the inlet gate could eventually be located.

(2) At the inlet node compute $\partial t_f/\partial x$ and $\partial t_f/\partial y$. The quantity $\partial t_f/\partial x$ is defined as the fill time sensitivity with respect to gate location in the x direction, and the term $\partial t_f/\partial y$ is defined as the fill time sensitivity with respect to gate location in the y direction.

(3) The search direction, from the steepest descent method, is now defined as

$$\begin{Bmatrix} -\dfrac{\partial t_f}{\partial x} \\ -\dfrac{\partial t_f}{\partial y} \end{Bmatrix}.$$

This is the gradient of the fill time with respect to the sensitivity parameter $\mathbf{x}$.

(4) Find a node along an edge intersected by the search direction. This point is used to make sure that the line segment searched does in fact have possible injection points at both ends.

(5) With the initial node location denoted as (x_1, y_1) and the point along the intersected edge denoted as (x_2, y_2), set

$$S = \begin{Bmatrix} x_2 - x_1 \\ y_2 - y_1 \end{Bmatrix},$$

where S defines the line segment used in the "golden section" method.

(6) Any point on S can be described by the function $\mathbf{x} + \lambda \cdot S$ where $\mathbf{x}$ is the initial position and λ is between 0 and 1.0. In the "golden section" method two points inside this range are then chosen for analysis; $\lambda_l = \lambda_{max} - \Phi \cdot (\lambda_{max} - \lambda_{min})$ and $\lambda_r = \lambda_{min} + \Phi \cdot (\lambda_{max} - \lambda_{min})$. These points are at a distance of $\Phi \cdot (\lambda_{max} - \lambda_{min})$ from each endpoint where $\Phi = \frac{1}{2}\left(\sqrt{5} - 1.0\right)$. When the results of the cost function are compared, the interval is then reduced by moving the minimum, λ_{min}, to the right, $\lambda_{min} = \lambda_l$, if the right value is less than the left value. If the left value is less than the right value, then it is obtained by moving the maximum λ_{max} to the left, $\lambda_{max} = \lambda_r$. This is continued until the minimum and maximum values are close enough, $\lambda_{max} - \lambda_{min} < \eta$, inside a specified tolerance at which time the "golden section" method is converged.

(7) Once the "golden section" method has been exhausted repeat the sensitivity analysis, until the "golden section" method converges to the original point, i.e. $\lambda = 0.0$. The optimized node is, therefore, the most recently analyzed point.

This procedure could be used for any sensitivity parameter but is most useful when multiple sensitivity parameters are analyzed together.

5. Numerical verification and examples

In this section the numerical developments are verified with analytical results and example of sensitivity results are given for a sample geometry.

5.1 Verification of isothermal RTM sensitivity equations

A circular disk with a hole (Figure 1(a)), being filled from the center with constant pressure is considered. The analytical fill time solution is given as (Mohan *et al.*, 1999):

$$t = \frac{\mu}{k}\frac{\Phi}{P_0}\left[\frac{R^2}{2}\ln\left(\frac{R}{R_0}\right) - \frac{R^2}{4} + \frac{R_0^2}{4}\right] \tag{44}$$

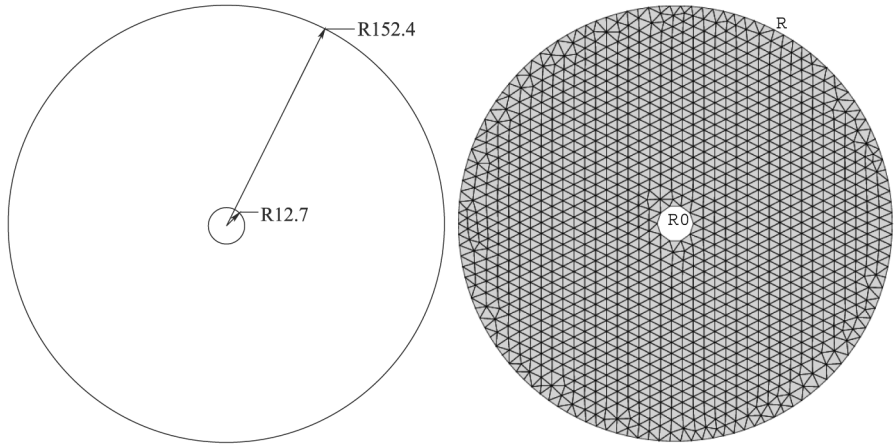

(a) Geometry **(b)** Finite element mesh

Figure 1.
Circular disk with hole (152.4 mm disk with a 12.7 mm hole) problem description for analytical/numerical comparison

where μ is the viscosity, Φ is the porosity, k is the permeability, P_0 is the inlet pressure, R_0 is the inner radius, R is the outer radius, and t is the time to fill from R_0 to R. The other possible inlet condition with an analytical solution is for the case of constant flow rate. This analytical solution for the flow front is given as (Mohan *et al.*, 1999):

$$R(t) = \left[\frac{Qt}{\pi \Phi H} + R_0^2\right]^{\frac{1}{2}} \tag{45}$$

where H is the mold thickness and Q is the inlet flow rate. The inlet pressure for the constant flow rate boundary condition can also be computed analytically, as

$$P_0 = \frac{\mu Q}{2\pi k H} \ln\left(\frac{R(t)}{R_0}\right) \tag{46}$$

where $R(t)$ is the radius filled to at a specific time. The analytical solution is employed to verify the isothermal filling solution. In addition, from these analytical solutions, sensitivity solution are also computed to validate the subsequent CSE developments for isothermal filling. The partial derivative of the fill time solution for constant inlet pressure, equation (44), with respect to the sensitivity parameter p, yields

$$\frac{\partial t}{\partial p} = \left(\frac{\partial \mu}{\partial p} \left(\frac{\Phi}{kP_0} \right) - \frac{1}{k^2} \frac{\partial k}{\partial p} \left(\frac{\mu \Phi}{P_0} \right) - \frac{1}{P_0^2} \frac{\partial P_0}{\partial p} \left(\frac{\mu \Phi}{k} \right) \right) \times \left[\frac{R^2}{2} \ln \left(\frac{R}{R_0} \right) - \frac{R^2}{4} + \frac{R_0^2}{4} \right] \quad (47)$$

The analytical sensitivity solution for a constant flow rate injection can also be derived from an analytical filling solution. Taking the partial derivative of equation (45) with respect to the sensitivity parameter p, yields

$$\frac{\partial t}{\partial p} = -\frac{1}{Q^2} \frac{\partial Q}{\partial p} [(R(t)^2 - R_0^2) \pi \Phi H] \quad (48)$$

For completeness the pressure sensitivity solution at the inlet is included for constant flow rate boundary conditions. The partial derivative of equation (46) with respect to the sensitivity parameter p, yields

$$\frac{\partial P_0}{\partial p} = \left(\frac{\partial \mu}{\partial p} \left(\frac{Q}{2\pi kH} \right) - \frac{1}{k^2} \frac{\partial k}{\partial p} \left(\frac{\mu Q}{2\pi H} \right) + \frac{\partial Q}{\partial p} \left(\frac{\mu}{2\pi kH} \right) \right) \ln \left(\frac{R(t)}{R_0} \right) \quad (49)$$

The verification of the isothermal sensitivity equations is performed by comparing the results from the analytical solution, equation (47), with the results obtained from the finite element RTM developments. The finite element mesh is shown in Figure 1(b). The material properties and boundary conditions employed for the simulations are listed in Table I. The results are presented in Figure 2(a) and (b). The comparative numerical and analytical results for inlet pressure and permeability sensitivities are shown in Figure 2(a) and (b), respectively. The agreement of the results is excellent and clearly verifies the present developments for sensitivity parameters of inlet pressure and permeability.

5.2 Fill time sensitivity problem description

Illustrative fill time sensitivity results are presented next for the 50.8 mm × 50.8 mm plate shown in Figure 3(a) and (b). The inlet location used for this model is the bottom left corner of the plate. The default model values for the results presented in Figures 4(a) and (b), 5(a) and (b), 6(a) and (b), are described in Table II.

Table I. Material properties and boundary conditions for the disk problem

$R_0 = 12.7$ mm	$R = 152.4$ mm	$\mu = 5.00$ cP
$k = 2.300 \times 10^{-12}$ m^2	$\Phi = 0.3$	vof $= 1.0 - \Phi = 0.7$
$P_0 = 689.5$ kPa		

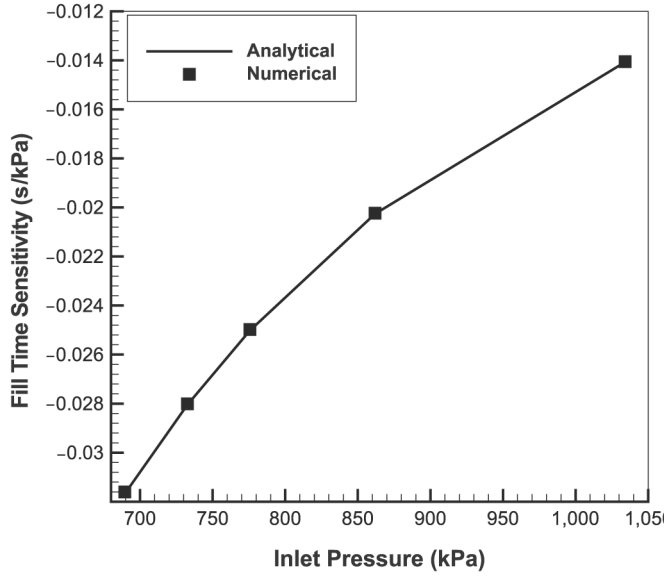

(a) Sensitivity parameter of inlet pressure

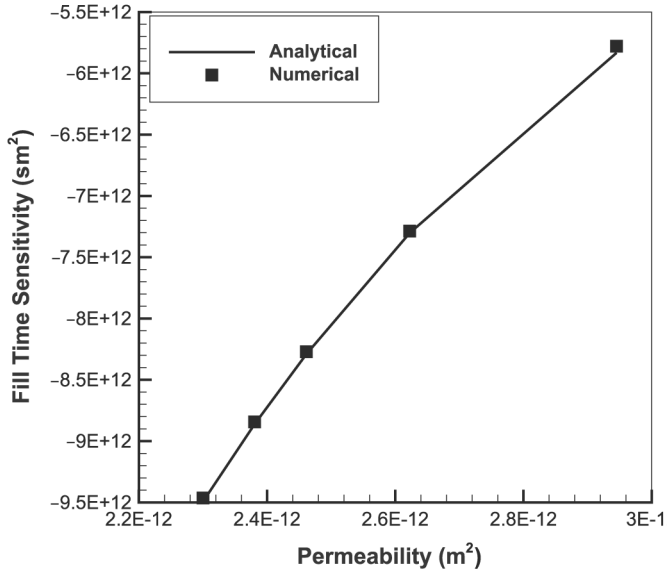

(b) Sensitivity parameter of permeability

Figure 2.
Comparison of analytical and numerical results for filling of the disk model

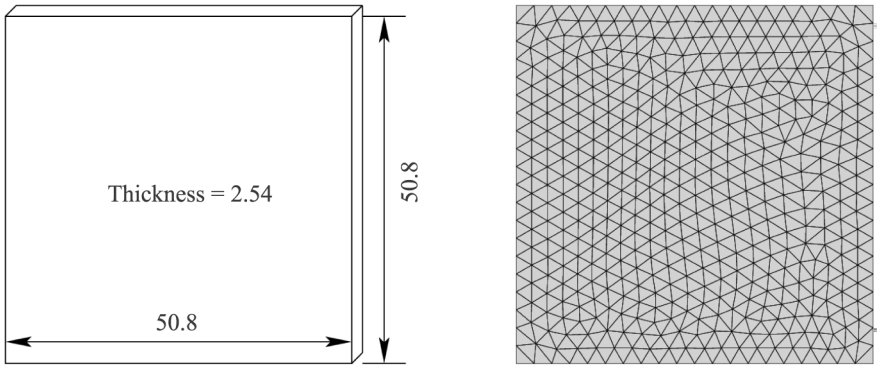

(a) Geometry **(b)** Finite element mesh

Figure 3.
Problem description of 50.8 mm × 50.8 mm plate filling problem

Inlet pressure, pressure sensitivity, fill time, and fill time sensitivity were computed. These results are shown as an illustration of the type of results one can obtain from utilizing the CSE. Note that the sensitivity values here are scaled using the method described in Blackwell *et al.* (1999a). In this method the sensitivity results are multiplied by the nominal parameter value as

$$\hat{S}_p = p_0 * S_p \tag{50}$$

where p_0 is the nominal parameter value. The sensitivity units in equation (50) are therefore the same as the model results, i.e. fill time and fill time sensitivity both have the same units. In Figure 4(a) the pressure and pressure sensitivity results are plotted for varying permeability values. The inlet pressure decreases with increasing permeability as would be expected from analysis of the analytical solution, (equation (46)). The absolute value of the pressure sensitivity decreases with increasing permeability, illustrating the fact that the inlet pressure is less sensitive to increase in permeability as the nominal value increases. Figure 4(b) plots the fill time and the fill time sensitivity versus permeability results. In Figure 4(b) the fill time decreases with increasing permeability as is expected from equation (47). Figure 5(a) and (b) shows the pressure and fill time sensitivity with respect to the resin viscosity. From the analytical solution, equation (44), it is evident that the fill time is directly proportional to the viscosity. The plots show this point. Since inlet pressure and fill time are directly proportional to the resin viscosity, the slope of the lines in Figure 5(a) and (b) are approximately constant and the sensitivity results have a slope of zero. Figure 6(a) shows inlet pressure and inlet pressure sensitivity versus inlet flow rate. The plots show the fact that inlet pressure is a linear function of inlet flow rate for this range of flow rates. Figure 6(b) shows the fill time and the fill time sensitivity results versus inlet pressure for

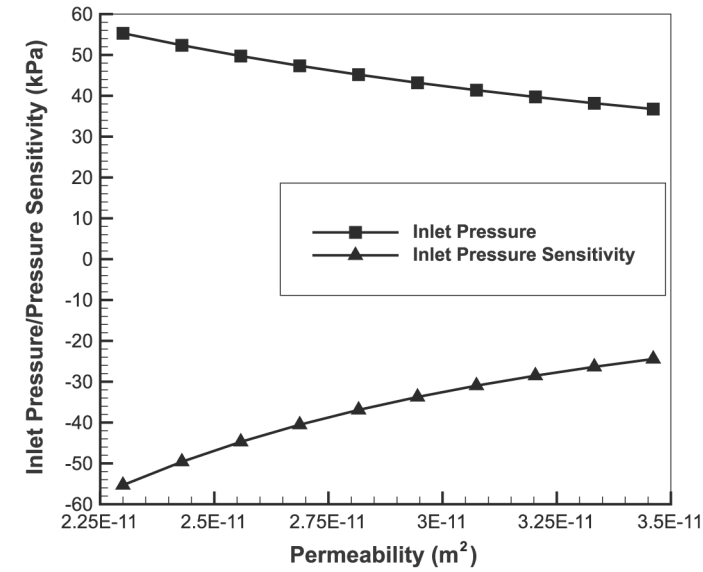

(a) Inlet pressure and inlet pressure sensitivity

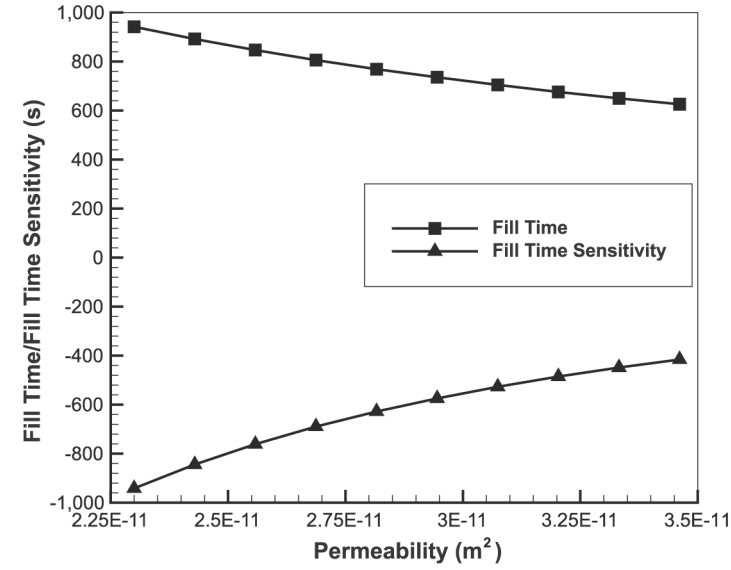

(b) Fill time and fill time sensitivity

Figure 4.
Sensitivity results vs permeability for the 50.8 mm × 50.8 mm flat plate

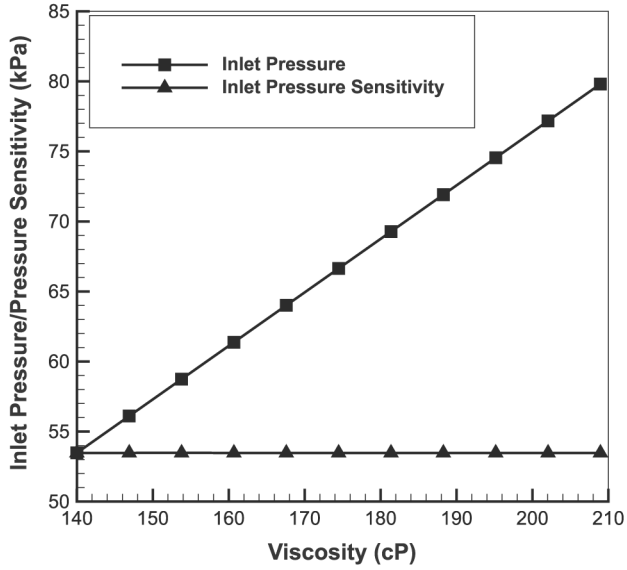

(a) Inlet pressure and inlet pressure sensitivity

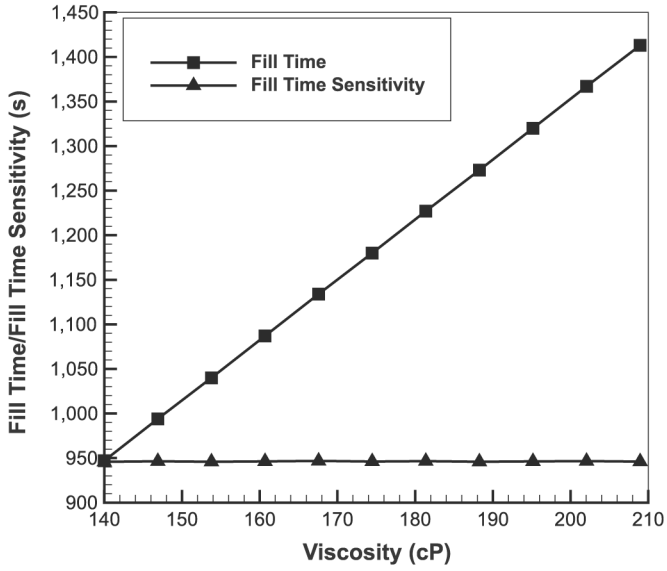

(b) Fill time and fill time sensitivity

Figure 5.
Sensitivity results vs viscosity for the 50.8 mm × 50.8 mm flat plate

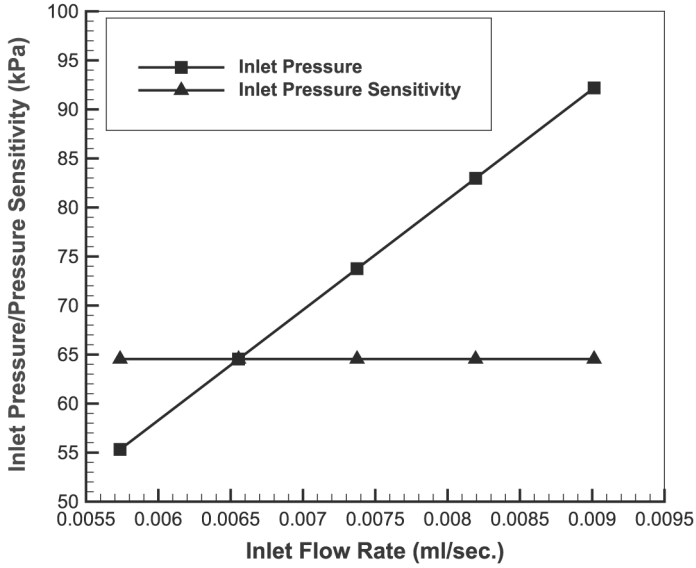

(a) Inlet pressure and inlet pressure sensitivity

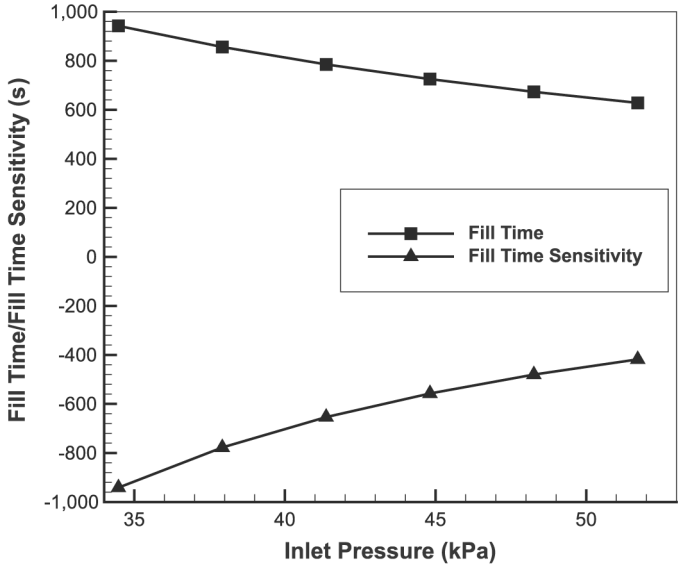

(b) Fill time and fill time sensitivity

Figure 6.
Sensitivity results vs inlet conditions for the 50.8 mm × 50.8 mm flat plate

the 50.8 mm × 50.8 mm plate. The trends of decreasing fill time and decreasing fill time sensitivity follow closely the analytical solutions given in equations (44) and (47), respectively. By combining all of the sensitivity results as a single plot, (Figure 7), and scaling the x-axis by the nominal value, it is possible to make some comments about each of the parameters with respect to each other. For instance, note that in Figure 7(a), at the nominal values chosen, the absolute values of all the pressure sensitivity results are similar, but as the values increase, permeability is less important to the maximum pressure in the mold. It is shown in Figure 7(b) that mold fill time is sensitive to a similar degree for all parameters but as the values increase fill time is less sensitive to inlet pressure and preform permeability than viscosity which remains constant.

5.3 Applications of the CSE

In this section, three applications of the CSE are demonstrated. These applications of the RTM CSE are unique in the literature for RTM. Another common application, minimization of fill time according to injection locations is also available (Mathur *et al.*, 2002).

5.3.1 Computation of unknown material property. In this sample illustrative problem the viscosity of flowing resin is assumed to be not accurately known for a particular structural part being manufactured. The numerical results are computed with the finite element discretized model and compared to the fill time measurements from the laboratory. The material properties and inlet conditions for the initial finite element model are selected as described in Table III.

The geometry and finite element model are shown in Figure 8(a) and (b), respectively. The model pertains to that termed as a risk reduction box geometry which has similarities to that of a typical keel beam for the Comanche helicopter.

The sensitivity results are used here to calculate the value of viscosity that was used in a laboratory experiment. During the experiment, mold filling occurred in approximately 60 s. Earlier a numerical analysis was performed using the FEM that predicted a fill time of approximately 100 s. By combining the sensitivity results with the Newton iteration method the unknown viscosity value is computed. The function to be solved is defined as

$$f(\mu) = t_{f_{\text{actual}}} - t_{f_{\text{simulated}}}(\mu) \tag{51}$$

In equation (51), $t_{f_{\text{actual}}}$ is the actual fill time measured in the laboratory, and $t_{f_{\text{simulated}}}(\mu)$ is the currently computed fill time from the finite element model.

Table II. Material properties and boundary conditions for the 50.8 mm × 50.8 mm plate problem

$k = 2.300 \times 10^{-11}\,\text{m}^2$	$\mu = 140.0\,\text{cP}$
$P_0 = 34.5\,\text{kPa}$	$q_0 = 5.735 \times 10^{-3}\,\text{ml/s}$

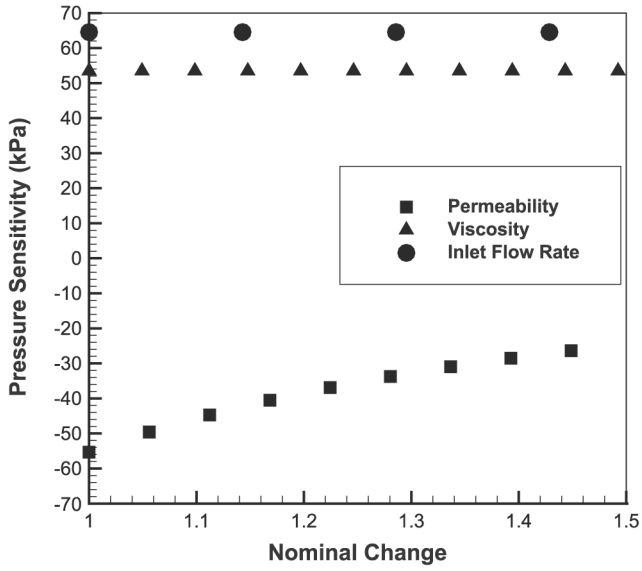

(a) Pressure sensitivity vs normalized parameter values

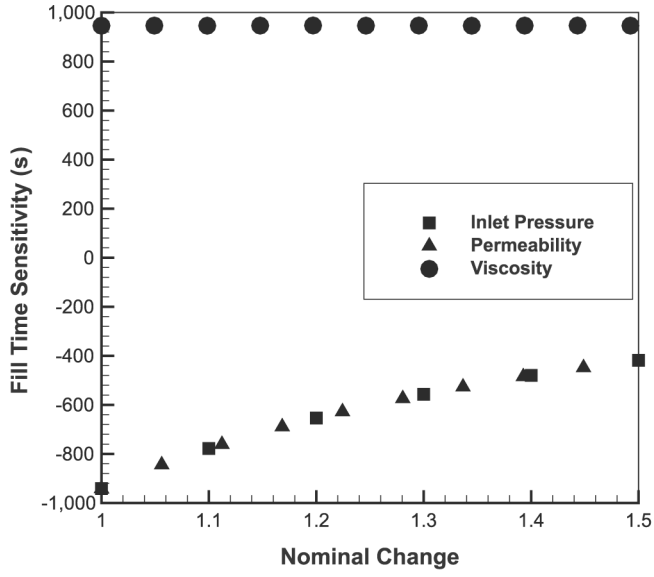

(b) Fill time sensitivity vs normalized parameter values

Figure 7.
Pressure and fill time sensitivity vs normalized parameter value plots for isothermal RTM filling of the 50.8 mm × 50.8 mm plate

By finding the root of this equation the viscosity from the experiment can be determined. To calculate the root of equation (51), the Newton method is used employing

$$\mu_{n+1} = \mu_n + \frac{-f(\mu_n)}{f'(\mu_n)} \tag{52}$$

where n denotes results from the previous viscosity estimation and n+1 denotes values for the current viscosity estimation. By iterating until convergence is reached the correct viscosity values are computed as shown graphically in Figure 9. Such techniques are of practical importance to designers and can also be applied to other analysis including fill time optimization, inlet parameter computations, etc.

5.3.2 Computation of multiple simultaneous unknown material properties. This example is similar to the previous example in that sensitivity results are used to compute unknown material properties. In this section experimental data are presented and compared to the simulation results. Sensitivity analysis can be employed to quantify and account for the variations in material properties that may exist during an actual experiment. This can be done using the measured data during the actual experiment as demonstrated here. The experimental front progression shows that the permeability tensor is not

Table III. Problem description

$k = 2.300 \times 10^{-12}\,\mathrm{m}^2$	$\mu = 5.00\,\mathrm{cP}$	$P_{\mathrm{inlet}} = 689.5\,\mathrm{kPa}$

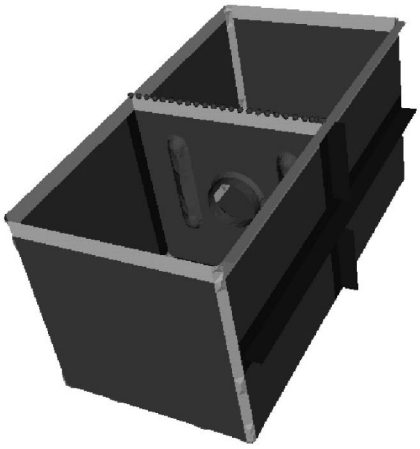

(a) Risk reduction box geometry with different material regions

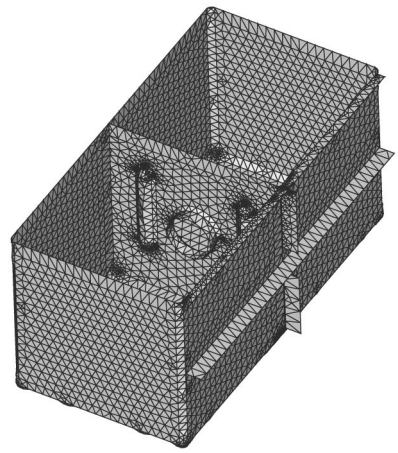

(b) Risk reduction box mesh

Figure 8. Geometry and finite element mesh used for computation of unknown material property

symmetric as initially assumed and therefore two material properties, namely, k_{xx} and k_{yy} are undetermined and need to be computed simultaneously. The experimental setup is mold filling of a 356 mm × 356 mm flat plate with a center injection gate. The simulations are based on experimentally measured viscosity and flow rate values. The initial permeability data employed in the simulations are based on a radial permeability setup as described in Table IV.

Pressure sensors were embedded into the fiber preform in order to measure the transient pressure history during filling. The locations of the pressure sensors are shown in Figure 10(a).

In the experiment the viscosity of the resin was measured prior to injection, so it is assumed that this value is accurate. The inlet flow rate is also measured during filling and precisely controlled. For isothermal filling this only leaves the permeability tensor as an unknown. The permeability of the actual preform inside a mold is difficult to know to an exact degree of certainty prior to injection. Permeability data based on separate radial flow experiments can be utilized but small changes in the way in which the fiber preform is set into the mold can affect the actual permeability tensor in the experimental setup.

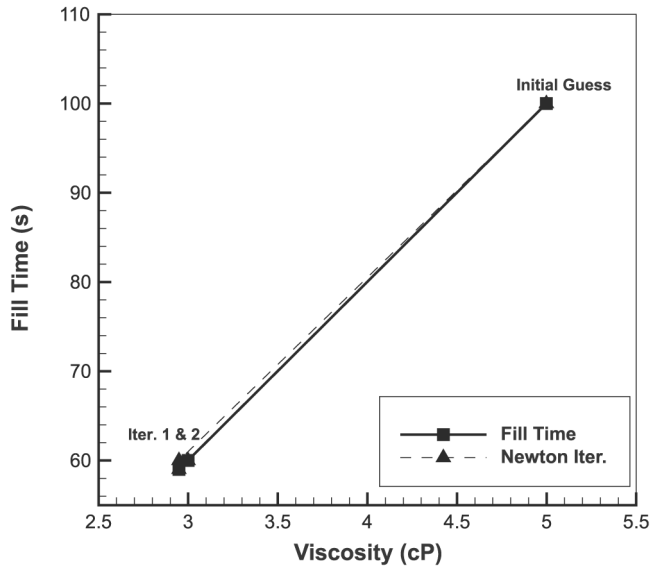

Figure 9.
Fill time vs viscosity with Newton iterations

Table IV.
Material properties and boundary conditions for the 356 mm × 356 mm plate problem

$k_{xx} = 4.70177899 \times 10^{-9}\,\mathrm{m}^2$	$k_{xy} = 0.0\,\mathrm{m}^2$	$k_{yy} = 4.70177899 \times 10^{-9}\,\mathrm{m}^2$
$\mu = 22.8\,\mathrm{cP}$	$q_{\mathrm{inlet}} = 9.552 \times 10^{-6}\,\mathrm{m}^3/\mathrm{s}$	Thickness = 3.175 mm

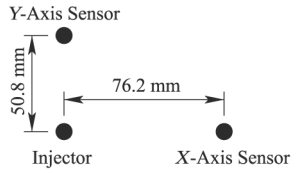

(a) Sensor locations

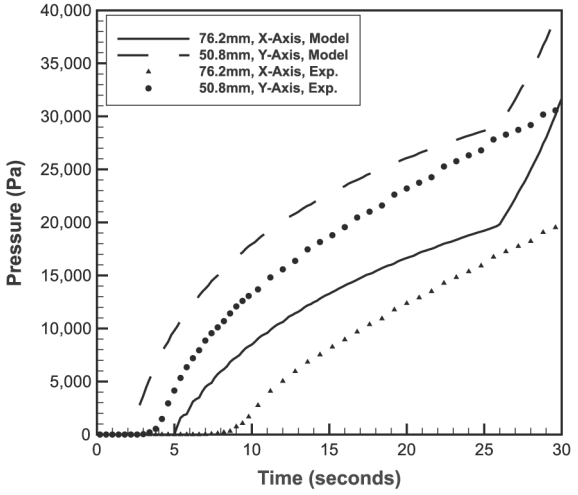

(b) Transient pressure history with the original permeability tensor

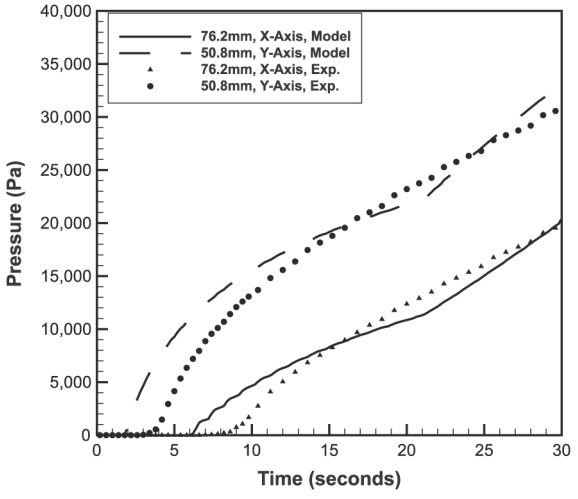

(c) Transient pressure history after sensitivity analysis with modified permeability tensor

Figure 10.
Comparison of experimental and simulated pressure data for 356 mm × 356 mm plate

The pressure during infusion is affected by the permeability tensor values and is a more rigorous parameter than flow front location. This example demonstrates application of sensitivity analysis discussed earlier to improve the accuracy and resolution of the permeability tensor using the experimentally measured parameters.

Based on the earlier discussions the permeability tensor is the only unknown in this example. Also, assuming that the major axes of the permeability tensor are the x and y directions, the off diagonal term, namely, k_{xy} is assumed to be zero, leaving only two unknowns. Since there are two unknowns there must be two independent equations available. The two equations used to compute the permeability tensor and improve the accuracy of the simulation are the following:

$$\begin{aligned} P_{\text{exp}} &= P_{\text{sim}} + \Delta k_{xx} S_{P_{k_{xx}}} + \Delta k_{yy} S_{P_{k_{yy}}} \quad \text{at point 1} \\ P_{\text{exp}} &= P_{\text{sim}} + \Delta k_{xx} S_{P_{k_{xx}}} + \Delta k_{yy} S_{P_{k_{yy}}} \quad \text{at point 2} \end{aligned} \tag{53}$$

where P_{exp} and P_{sim} are the experimental and simulated pressure values at the pressure sensors, respectively. $S_{P_{kxx}}$ and $S_{P_{kyy}}$ are the pressure sensitivity values with respect to the k_{xx} and k_{yy} permeability tensor terms, respectively. After solving for Δk_{xx} and Δk_{yy} in equation (53) the new permeability tensor is input to the simulation and new pressure results are computed. With the filling being a transient problem and an experimental transient pressure history available, equation (53) is solved at various stages of filling and the average changes in k_{xx} and k_{yy} values are determined. In this example equation (53) is solved at five different transient times during filling. This process continues until convergence. The final computed permeability tensor values for this model are given as

$$k_{xx} = 5.00814899 \times 10^{-9}; \quad k_{xy} = 0.0; \quad k_{yy} = 7.58130899 \times 10^{-9}\,\text{m}^2$$

These values are input to the simulation and the transient pressure history at the pressure sensor locations is computed. The results for the simulations with initial permeability values and sensitivity modified values are compared in Figure 10. Figure 10 shows that there is significant deviation in the simulated pressure histories compared with the experimental data. After iterating using equation (53) until convergence, the pressure data with the new sensitivity modified permeability tensor shows a much better agreement with the experimental results. Equation (53) is solved for five predetermined times (6, 12, 18, 24, and 28.8 s) during each simulation. The average computed permeability is then used for the next iteration. The pressure at the injector location was measured in the experiment and also computed in the finite element model. Figure 11 shows the comparison of injection pressures. The injection pressure histories with the sensitivity modified permeability tensor shows significant

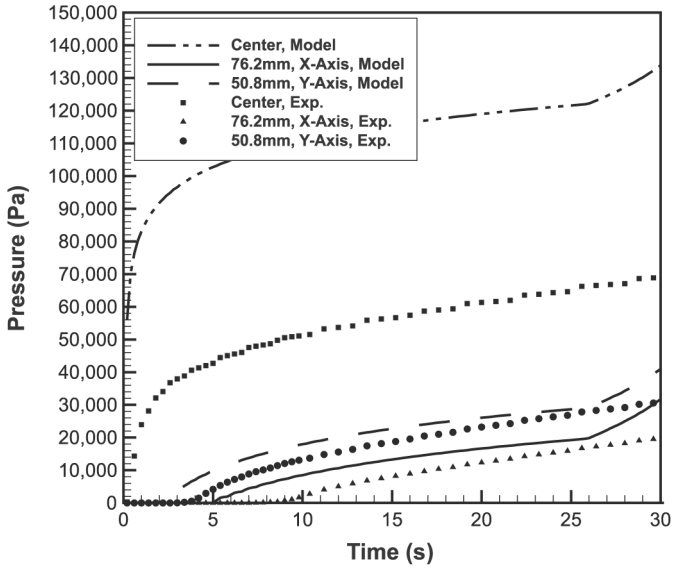

(a) Transient pressure history with original permeability tensor

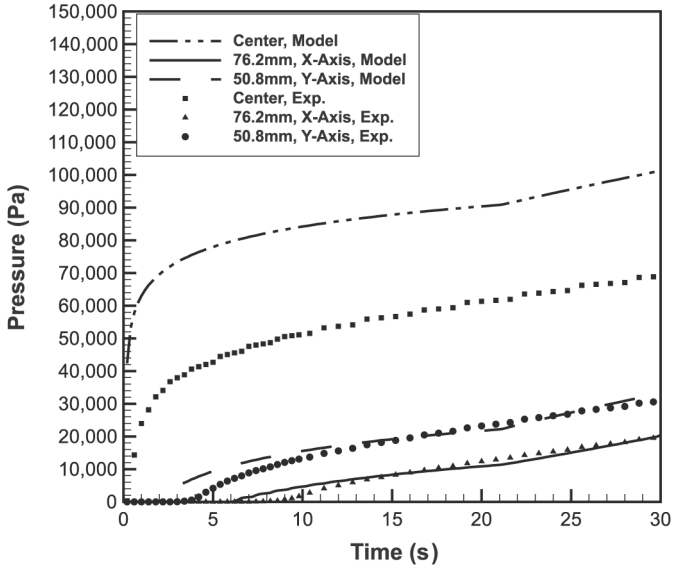

(b) Transient pressure history with sensitivity modified permeability tensor

Figure 11. Comparison of experimental and simulated pressure data for 356 mm × 356 mm plate including pressure at the injection location

improvement over the initial permeability tensor. An equation similar to equation (53) with the injector pressure is not included when computing the permeability tensor because the pressure measured in the experiment can be inaccurate at the injector location. Also, the pressure results computed in the finite element model are highly sensitive to the mesh size around the injector which leads to inaccuracy. The plots in Figure 11 are included to show that the trend observed in the injector is indeed consistent between the experimental data and the simulation data, in both cases with improved accuracy in the comparisons.

5.3.3 Optimization of a boundary condition. Obtaining the minimum possible fill time for a particular mold is important in keeping manufacturing costs down. A constant flow rate injection allows for control over mold filling at the expense of minimum fill time. If the mold pressure can not exceed some predetermined value it would be useful to be able to predict what the maximum flow rate would be to stay under this threshold value. Sensitivity analysis combined with the Newton iteration method can be used to predict this maximum flow rate and thus optimize the mold filling process. In equations (51) and (52) μ is replaced by inlet flow rate q_0. In this example, the complex part in Figure 12 is used. Note that in Figure 13 only three iterations after the initial guess are required to compute an inlet flow rate that should result in a pressure below the threshold value. The minimum fill time required for this mold with predetermined inlets and vents can be simulated by applying a constant pressure boundary condition at the inlets. A constant pressure injection may not be the most desirable although the control over the resin flow is important for manufacturing quality parts.

6. Concluding remarks

A wide variety of parametric investigations to include material property, boundary conditions, and geometric sensitivity parameters and analysis

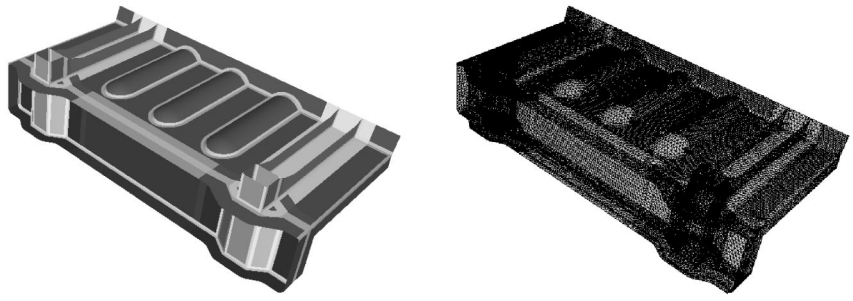

(a) Complex composite geometry with different material regions

(b) Complex composite part mesh

Figure 12.
Geometry and finite element mesh used in optimization study

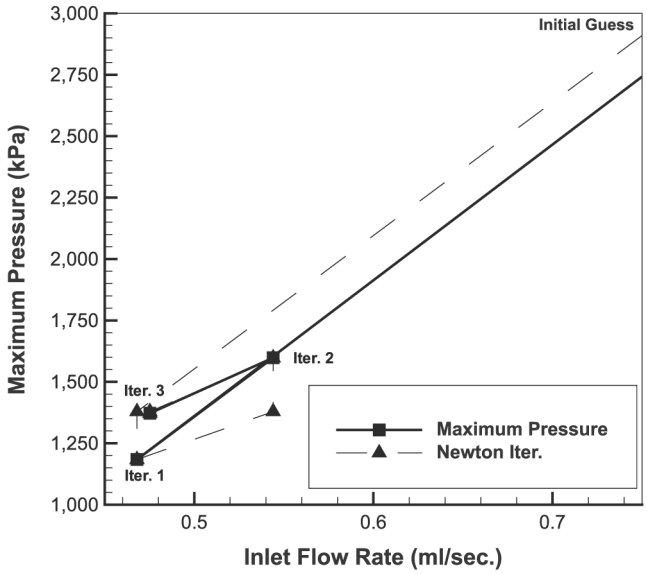

Figure 13.
Maximum pressure vs inlet flow rate with Newton iterations

studies were presented for isothermal RTM considerations. The CSE was developed for the isothermal RTM process simulation studies by starting from the governing model equations and applying the FEM. Once the CSE was formulated, a cost function, namely the fill time, was derived along with the fill time sensitivity. Using analytical results for filling of a disk the numerical developments were verified for sensitivity analysis. A simple 50.8 mm square plate and the corresponding sensitivity results were presented. A sample application for the sensitivity results was given in the computation of an unknown material property of a structural part manufactured by RTM process. In the analysis the viscosity was computed for the geometry of a risk reduction box after example laboratory results did not coincide with the results from the numerical simulations. Optimization of a boundary condition value was also presented as an application of the CSE. The usefulness of the present efforts as a design tool was subsequently demonstrated.

References

Blackwell, B.F., Dowding, K.J. and Cochran, R.J. (1999a), "Development and implementation of sensitivity coefficient equations for heat conduction problems", *Numerical Heat Transfer, Part B*, Vol. 36, pp. 15-32.

Blackwell, B.F., Dowding, K.J. and Cochran, R.J. (1999b), "Application of sensitivity coefficients for heat conduction problems", *Numerical Heat Transfer, Part B*, Vol. 36, pp. 33-55.

Chui, W.K., Glimm, J., Tengerman, F.M., Jardine, A.P., Madsen, J.S., Donnellan, T.M. and Leek, R. (1997), "Process modeling in resin transfer molding as a method to enhance product quality", *Society for Industrial and Applied Mathematics*, Vol. 39 No. 4, pp. 714-27.

Gantar, G. and Kuzman, K. (2002), "Sensitivity and stability evaluation of the deep drawing process", *Journal of Materials Processing Technology*, Vols. 125-126, pp. 302-8.

Gelin, J.C. and Labergere, C. (2002), "Application of optimal design and control stategies to the forming of thin walled metallic components", *Journal of Materials Processing Technology*, Vols. 125-126, pp. 565-72.

Ghouati, O., Lenoir, H. and Gelin, J.C. (2000), "Optimal design of forming processes using the finite element method", *Advanced Engineering Materials*, Vol. 2 No. 7, pp. 438-42.

Henz, B.J., Kanapady, R., Ngo, N., Chung, P. and Tamma, K.K. (2000), "Simulation based design and visualization tools: sensitivity coefficients for advanced composites manufacturing", *AHPCRC Bulletin*, Vol. 10, pp. 18-20.

Henz, B.J., Tamma, K.K., Kanapady, R., Ngo, N.D. and Chung, P.W. (2002), "Process modeling of composites by resin transfer molding: sensitivity analysis for isothermal considerations", *AIAA-2002-0790, 41st Aerospace Sciences Meeting*, Reno, NV, January 2002.

Jiang, S., Zhang, C. and Wang, B. (2001), "A process performance index and its application to optimization of the RTM process", *Polymer Composites*, Vol. 22 No. 5, pp. 690-701.

Kim, B.Y., Nam, G.J. and Lee, J.W. (2002), "Optimization of filling process in RTM using a genetic algorithm and experimental design method", *Polymer Composites*, Vol. 23 No. 1, pp. 72-86.

Mathur, R., Advani, S.G. and Fink, B.K. (2002), "A sensitivity-based gate location algorithm for optimal mold filling during the resin-transfer molding (RTM) process", *Tech. Rep. ARL-TR-2771*, US Army Research Laboratory, Aberdeen Proving Grounds, Aberdeen Proving Ground, MD.

Mohan, R.V., Ngo, N.D. and Tamma, K.K. (1999), "On a pure finite element methodology for resin transfer mold filling simulations", *Polymer Engineering and Science*, Vol. 39 No. 1, pp. 26-43.

Mohan, R.V., Shires, D.R., Tamma, K.K. and Ngo, N.D. (1998), "Flow channels and fiber impregnation studies for the process modeling/analysis of complex engineering structures manufactured by resin transfer molding", *Polymer Composites*, Vol. 19 No. 5, pp. 527-42.

Navarrina, F., López-Fontán, S., Colominas, I., Bendito, E. and Casteleiro, M. (2000), "High order shape design sensitivity: a unified approach", *Computer Methods in Applied Mechanics and Engineering*, Vol. 188, pp. 681-96.

Ngo, N.D., Mohan, R.V., Chung, P.W. and Tamma, K.K. (1998), "Recent developments encompassing non-isothermal/isothermal liquid composite molding process modeling/analysis: physically accurate, computationally effective and affordable simulations and validations", *Journal of Thermoplastic Composite Materials*, Vol. 11 No. 6, pp. 493-532.

Press, W.H., Teukolsky, S.A., Vetterling, W.T. and Flannery, B.P. (2002), *Numerical Recipes in C++*, Cambridge University Press, Cambridge, UK.

Shewchuk, J.R. (1994), "An introduction to the conjugate gradient method without the agonizing pain", *Tech. rep.*, Carnegie Mellon University, Pittsburgh, PA.

Further reading

Bruschke, M.V. and Advani, S.G. (1990), "A finite element/control volume approach to mold filling in anisotropic porous media", *Polymer Composites*, Vol. 11, pp. 398-405.

Fracchia, C.A., Castro, J., Tucker, C.L. (1989), "A finite element/control volume simulation of resin transfer mold filling", The American Society For Composites, *4th Technical Conference*, 157-66.

Hirt, C.W. and Nichols, B.D. (1981), "Volume of fluid method for the dynamics of free boundaries", *Journal of Computational Physics*, Vol. 39, pp. 201-25.

Huebner, K.H., Thorton, E.A. and Byrom, T.G. (1995), *The Finite Element for Engineers*, Wiley, New York, NY.

Hwang, W.S. and Stoehr, R.A. (1988), "Molten metal flow pattern prediction for complete solidification analysis of near net shape castings", *Materials Science and Technology*, Vol. 4, pp. 240-50.

Mohan, R.V., Ngo, N.D. and Tamma, K.K. (1999a), "Three-dimensional resin transfer molding: part 1 – isothermal process modeling and explicit tracking of moving fronts for thick geometrically complex composites manufacturing applications", *Numerical Heat Transfer, Part A – Applications*, Vol. 35 No. 8, pp. 815-38.

Mohan, R.V., Ngo, N.D., Tamma, K.K. and Shires, D.R. (1999b), "Three-dimensional resin transfer molding: part 2 – isothermal process modeling and implicit tracking of moving fronts for thick geometrically complex composites manufacturing applications", *Numerical Heat Transfer, Part A – Applications*, Vol. 35 No. 8, pp. 839-58.

Pelletier, D., Borggaard, J. and Hetú, J-F. (2000), "A continuous sensitivity equation method for conduction and phase change problems", *38th AIAA Aerospace Sciences Meeting and Exhibit*, Reno, NV, 10-13 January 2000, American Institute of Aeronautics and Astronautics, Reston, VA.

Trouchu, F., Gauvin, R. and Gao, D.M. (1993), "Numerical analysis of the resin transfer molding process by the finite element method", *Advances in Polymer Technology*, Vol. 12, pp. 329-42.

Usmani, A.S., Cross, J.T. and Lewis, R.W. (1992), "A finite element model for the simulations of mold filling in metal casting and the associated heat transfer", *International Journal of Computational Physics*, Vol. 35, pp. 787-806.